A discrete particle contact model for sintering

S. Luding
Particle Technology, DelftChemTech, TU Delft, Julianalaan 136, 2628 BL Delft, Netherlands

ABSTRACT: A discrete model for the sintering of discrete particles in two dimensions is presented with empirical contact force-laws, taking into account plastic deformations, cohesion, temperature dependence (melting and freezing), and also long-time relaxation effects. Samples are prepared under constant isotropic load, and are sintered for different sintering times. During sintering, the sample shrinks, i.e. becomes denser with increasing sintering time. Both increasing external load and sintering time lead to a stronger, stiffer sample after cool-down. With a compression test, the sample is destroyed via vertical cracks opening.

1 INTRODUCTION

There are two ways to describe and model a particulate, inhomogeneous material like powder, ceramics or concrete. The first approach is based on continuum theory and relies on empirical assumptions about the macroscopic material behavior (Schwedes 1968; Olevsky 1998; Vermeer, Diebels, Ehlers, Herrmann, Luding, and Ramm 2001; Riedel and Blug 2001; Luding, Manetsberger, and Müllers 2004). This macroscopic approach is complemented by a "microscopic" description of the material on the particle or grain level where the particles and their interactions are modeled one by one using so-called discrete element methods (DEM) (Herrmann, Hovi, and Luding 1998; DeLo, Dutton, and Semiatin 1999; Vermeer, Diebels, Ehlers, Herrmann, Luding, and Ramm 2001). The former involves stress, strain and plastic yield conditions (Redanz and Fleck 2001), whereas the latter deals with local force-deformation laws for each contact (Jagota and Dawson 1990; Luding, Manetsberger, and Müllers 2004).
The microscopic interaction model for plastic deformations, friction, and cohesion is discussed and time-, temperature-, and history dependent behavior is introduced and rationalized. After definition of the contact force laws, a model system in a two-dimensional box filled with disks of different sizes, is examined by means of DEM.

2 MODEL SYSTEM

The numerical "experiment" chosen is a bi-axial box set-up, see [S. Luding et al., in this volume], where the left and bottom walls are fixed, and a stress- or strain-controlled deformation is applied to the other walls. In the future, quantitative agreement between experiment and simulation has to be achieved, however, this issue is far from the scope of this paper where, mainly, the new contact model is proposed.

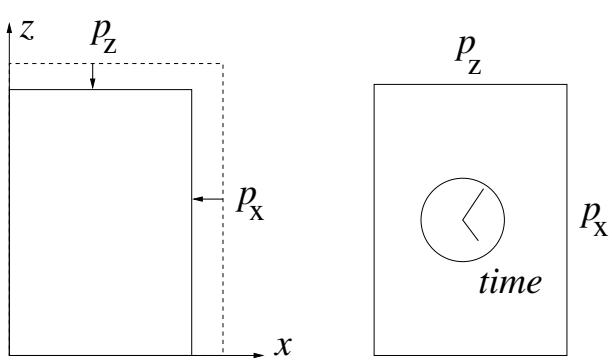

Figure 1. (Left) Preparation of the sample with pressure on both sides. (Right) After the system is relaxed the evolution in time of the sample with time is examined.

Inside the system, N disks with radii a_i ($i = 1, \ldots, N$) and height h are placed. The radii are drawn from a homogeneous distribution with mean a_0 and relative width w_0 so that $a_i/a_0 \in [1 - w_0, 1 + w_0]$. The particle-particle interactions and the parameters involved are discussed in the next section.

3 DISCRETE PARTICLE MODEL

The elementary units of granular materials are mesoscopic grains which deform under stress, possibly yield, change their properties with time, and can behave different for different temperatures. Since the realistic modeling of the deformations of the particles is much too complicated to allow for a subsequent many-particle simulation, we relate the interaction force to the overlap δ of two particles. In the absence of long-range forces, an interaction takes place only if particles are in contact and thus $\delta > 0$. In that case, the forces are split into a normal and a tangential component denoted by n and t, respectively.

If all forces $\boldsymbol{f}_i$ acting on the particle i, either from other particles, from boundaries or from external forces, are known, the problem is reduced to the integration of Newton's equations of motion for the translational and rotational degrees of freedom. The integration of the equations of motion is performed with the simplest molecular dynamics Verlet algorithm together with Verlet-table neighborhood search (Allen and Tildesley 1987) – this is done in order to proof that the contact model is stable (given a small enough integration time-step) and does not rely on advanced algorithms.

3.1 Normal Contact Model

Two particles i and j at positions $\boldsymbol{r}_i$ and $\boldsymbol{r}_j$, with radii a_i and a_j, interact only if they are in contact so that their overlap

$$\delta = (a_i + a_j) - (\boldsymbol{r}_i - \boldsymbol{r}_j) \cdot \boldsymbol{n} \tag{1}$$

is positive, $\delta > 0$, with the unit vector $\boldsymbol{n} = \boldsymbol{n}_{ij} = (\boldsymbol{r}_i - \boldsymbol{r}_j)/|\boldsymbol{r}_i - \boldsymbol{r}_j|$ pointing from j to i. The force on particle i, from particle j can be written as $\boldsymbol{f}_{ij} = f^n_{ij}\boldsymbol{n} + f^t_{ij}\boldsymbol{t}$, with $\boldsymbol{n}$ perpendicular to $\boldsymbol{t}$. In this subsection, the normal forces are discussed.

3.1.1 Short time contact model

As first step, we discuss the time- and temperature-independent behavior of the contact forces between a pair of particles. For this, we modify and extend the linear hysteretic spring model (Walton and Braun 1986; Luding 1998; Tomas 2000). It is the simplest version of some more complicated nonlinear-hysteretic force laws (Walton and Braun 1986; Zhu, Shukla, and Sadd 1991; Sadd, Tai, and Shukla 1993), which reflects the fact that at the contact point, plastic (permanent) deformations may take place. The repulsive (hysteretic) force can be written as

$$f_{ij} = \begin{cases} k_1\delta & \text{loading,} \\ k_2(\delta - \delta_0) & \text{un/reloading,} \\ -k_c\delta & \text{unloading,} \end{cases} \tag{2}$$

with $k_1 \leq k_2$, see Fig. 2.

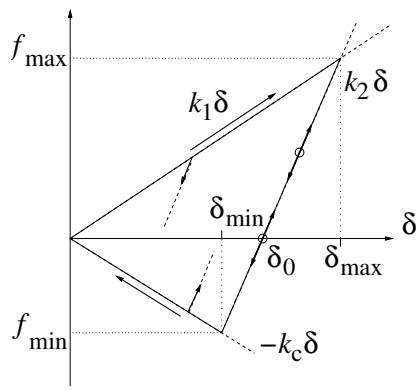

Figure 2. Force law for two springs with stiffness k_1 and k_2 for initial loading and subsequent un/reloading, respectively. Attractive forces are possible due to the cohesion strength k_c.

During the initial loading the force increases linearly with the overlap δ, until the maximum overlap $\delta_{\max}$ is reached, which is kept in memory as a *history parameter*. The line with slope k_1 thus defines the maximum force possible for a given δ. During unloading the force drops, on the line with slope k_2, from its value at $\delta_{\max}$ down to zero at the force-free overlap

$$\delta_0 = (1 - k_1/k_2)\delta_{\max} \ .$$

Reloading at any instant leads to an increase of the force along this line, until the maximum force is reached; for still increasing δ, the force follows again the line with slope k_1 and $\delta_{\max}$ has to be adjusted accordingly. Unloading below δ_0 leads to negative, attractive forces until at the overlap

$$\delta_{\min} = \frac{k_2 - k_1}{k_2 + k_c}\delta_{\max} \ ,$$

the minimum force $f_{\min} = -k_c\delta_{\min}$, i.e. the maximum attractive force, is obtained as a function of the model parameters k_1, k_2, k_c, and the history parameter $\delta_{\max}$. Further unloading leads to attractive forces on the branch $f = -k_c\delta$. The highest possible attractive force, for given k_1 and k_2, is reached for $k_c \to \infty$, so that $f_{\min} = -(k_2 - k_1)\delta_{\max}$. This would lead to a discontinuity at $\delta = 0$ that is avoided by using finite k_c.

The cone formed by the lines with slope k_1 and $-k_c$ defines the range of possible force values. If a force would fall outside the cone, it is forced to remain on the limit lines. Departure from these lines into the cone takes place in the case of unloading and reloading, respectively. Between these two extremes, unloading and reloading follow the same line with slope k_2. Possible equilibrium states are indicated as circles in Fig. 2, where the upper and lower circle correspond to a pre-stressed and stress-free state, respectively.

3.1.2 Viscous dissipation

In the case of collisions of particles and for large deformations, dissipation takes place due to the hysteretic nature of the force-law. For small displacements around some equilibrium state, the model does not contain strong dissipation. Therefore, in order to allow for stronger dissipation and thus faster relaxation, a viscous, velocity dependent dissipative force in normal direction,

$$f_{ij}^{n,\mathrm{d}} = \gamma_0 \dot{\delta} \ , \tag{3}$$

is assumed with some damping coefficient γ_0. The half-period of a vibration around the equilibrium position, see Fig. 2, can be computed for arbitrary values of k_1 and k_c, as long as the overlap fulfills the condition $\delta_{\mathrm{min}} < \delta < \delta_{\mathrm{max}}$. In this case, k_2 determines the stiffness and one obtains a typical response time on the contact level (Luding 1997),

$$t_c = \frac{\pi}{\omega} \ , \quad \text{with} \quad \omega = \sqrt{\frac{k_2}{m_{12}} - \eta_0^2} \ , \tag{4}$$

the eigenfrequency of the contact, the rescaled damping coefficient $\eta_0 = \gamma_0/(2m_{12})$, and the reduced mass $m_{12} = m_1 m_2/(m_1 + m_2)$. The time-step of the simulation t_{MD} has to be chosen such that

$$t_{\mathrm{MD}} \approx t_c/50$$

for a proper integration of the equations of motion, so that we chose a typical time-step $t_{\mathrm{MD}} = \pi/(50\omega)$ after the model parameters k_2 and γ_0 are specified

3.1.3 Stiffness increase with contact area

In order to account for the fact that a larger contact surface leads to a larger contact stiffness, the coefficient k_2 is made dependent on the maximum overlap history parameter δ_{max} (and thus on the force-free overlap δ_0), as long as the overlap is below the threshold δ^{fluid} that corresponds to the "complete melting" of the particles (Luding, Manetsberger, and Müllers 2004).

The stiffness is maximal in the fluid limit for $\delta_0 = \delta^{\mathrm{fluid}}$, which corresponds to $\delta_{\mathrm{max}} = \delta_{\mathrm{max}}^{\mathrm{fluid}} = k_2\delta^{\mathrm{fluid}}/(k_2 - k_1)$, and varies between k_1 and k_2 for smaller overlaps, so that

$$k_2(\delta_{\mathrm{max}}) = \begin{cases} k_2 & \text{if } \delta_{\mathrm{max}} \geq \delta_{\mathrm{max}}^{\mathrm{fluid}} \\ k_1 + (k_2 - k_1)\frac{\delta_{\mathrm{max}}}{\delta_{\mathrm{max}}^{\mathrm{fluid}}} & \text{if } \delta_{\mathrm{max}} < \delta_{\mathrm{max}}^{\mathrm{fluid}} \end{cases} \tag{5}$$

For large overlaps (in the fluid regime), the stiffness and the force is thus only dependent on k_2, independent of k_1. For smaller overlaps both k_1 and k_2 affect the force together with the history of this contact.

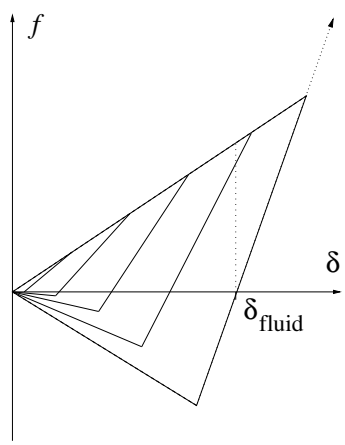

Figure 3. Force law with varying stiffness $k_2(\delta_{\mathrm{max}})$. If δ_0 becomes larger than δ^{fluid}, the stiffness remains equal to k_2.

The hysteretic stiffness model takes into account an increasing stiffness with increasing overlap. The first loading is plastic with low stiffness, and subsequent un- and reloading are stiffer because the material was initially compressed. Thus, also the maximum cohesive force depends on the maximum compression which was experienced by the contact during its history.

3.2 Density Temperature Dependence

If a solid (we assume a simple material here), is heated, in general, its volume increases so that its density decreases. Therefore, we assume a temperature dependent density of the single particles (disks with radius a and height h):

$$\rho(T) = \frac{m}{\pi a^2 h} = \rho(T_{\mathrm{melt}}) + \delta\rho_T\,(T_{\mathrm{melt}} - T) \ , \tag{6}$$

with the density change per unit temperature $\delta\rho_T$. This corresponds (in linear approximation) to a change of the particle radius

$$a(T) = a(T_{\mathrm{melt}})[1 - \delta a_T\,(T_{\mathrm{melt}} - T)] \ , \tag{7}$$

with the relative change of the radius per unit temperature δa_T. This approximation can be used if the range of temperatures is rather narrow and the changes per unit temperature are very small.

3.3 Contact Temperature Dependence

For the temperature dependence, we focus on an inhomogeneous material with a melting temperature T_{melt} and assume that the material behaves static, as described above, if the temperature T is much smaller than the melting temperature. The behavior of the stiffness k_1 is schematically shown in Fig. 4 as a function of the temperature.

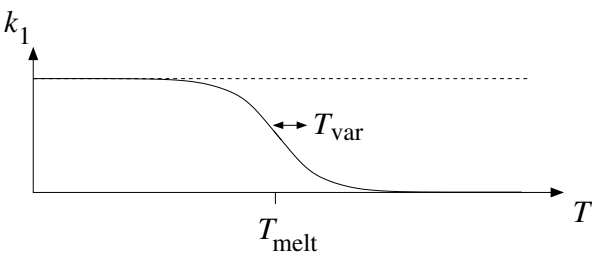

Figure 4. Schematic plot of the stiffness k_1 as a function of the temperature.

The material becomes softer when $T_{\text{melt}} - T$ becomes small and will lose all stiffness in the limit $T \gg T_{\text{melt}}$. The temperature range in which the melting takes place is quantified by T_{var}. In the transition regime $|T_{\text{melt}} - T| \approx T_{\text{var}}$, the particles are significantly softer than in the *cold* limit $T_{\text{melt}} - T \gg T_{\text{var}}$, and in the *hot* and the liquid regime, $T - T_{\text{melt}} \gg T_{\text{var}}$, one has $k_1 \to 0$ and the particles should behave "liquid" with considerable overlap.

3.3.1 Increasing temperature

When the temperature is increased to a rather large value, close to the melting point, two particles under stress and in equilibrium due to compressive forces will lose stiffness and thus will deform stronger so that their overlap becomes larger. Therefore, we assume for the stiffness coefficient

$$\begin{aligned} k_1(T) &= \frac{k_1}{2}\left[1 + \tanh\left(\frac{T_{\text{melt}} - T}{T_{\text{var}}}\right)\right] \\ &= \frac{k_1}{2}\left[1 + \tanh(\tau)\right] , \end{aligned} \tag{8}$$

with the dimensionless temperature difference τ. When k_1 is reduced due to an increase in temperature (+), we assume that δ^+_{max} remains constant, so that one obtains a larger force-free overlap $\delta^+_0(T) = [1 - k_1(T)/k_2(\delta^+_{\text{max}})]\delta^+_{\text{max}}$. Thus the material volume shrinks due to sintering (increasing overlap) at the contact level. Note that k_2 is not changed directly when T is increased.

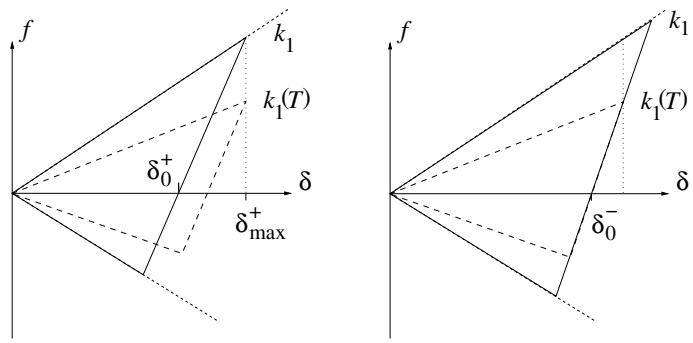

Figure 5. Force laws for varying stiffness k_1, according to Eq. (8). (Left) Temperature increase: k_1 is reduced while δ^+_{max} remains constant (dashed line, stress-free case). (Right) Temperature decrease:, k_1 is increased while δ^-_0 remains constant (solid line with slope k_2).

If, as an example, the material has a melting point $T_{\text{melt}} = 120^0$C with a range of softening of $T_{\text{var}} = 10^0$C, for a temperature of 122^0C, the stiffness is only 0.4 of the cold limit.

3.3.2 Decreasing temperature

If, later in time, the temperature is decreased again, $k_1(T)$ is adjusted according to Eq. (8), but since the melted (sintered) area around the contact point will not return to its previous state, we now assume that $\delta^-_0 =$ const., so that the maximum overlap increases to the value $\delta^-_{\text{max}}(T) = \delta^-_0/[1 - k_1(T)/k_2]$, see the right panel in Fig. 5.

The temperature dependence thus can lead to changes of the stiffness and of the overlap (deformation) of the particles.

3.4 Temperature dependence with time

In addition to the direct effect of a temperature change on the particle size and the stiffness, the material may change its internal, atomistic structure such that, e.g., defects heal and disappear. This effect will occur mainly in the regime of higher temperatures. Therefore, a time dependence is introduced that leads to an explicit change of the material stiffness k_1 with time. The change takes place extremely slowly with an *algebraic* time dependence, so that $k_1(T, t)$ lags behind when varying from its actual value to the desired, final value $k_1(T)$, as defined in the above equation (8).

When the temperature is increased from a small value T_0 to T, then $k_1(T_0)$ changes to $k_1(T)$ with the

rate of change

$$\frac{\partial k_1(T,t)}{\partial t} = \pm \frac{[k_1(T) - k_1(T,t)]^2}{k_1(T)\, t_0} \ , \qquad (9)$$

with the time scale t_0 on which a typical change takes place. Note that k_1, $k_1(T)$, and $k_1(T,t)$ are different, in general, and correspond to the maximum k_1, the temperature dependent $k_1(T) < k_1$, and the time dependent $k_1(T,t)$ that tends towards $k_1(T)$. The sign in Eq. (9) is chosen according to the sign of $[k_1(T) - k_1(T,t)]$.

Assume $T_0 = 20^0$C and $T = 118^0$C, so that $k_1(T_0) = 1$ corresponds to $k_1(T) = 0.6$. The stiffness as a function of time is plotted in Fig. 6 for the time constant $t_0 = 10$s.

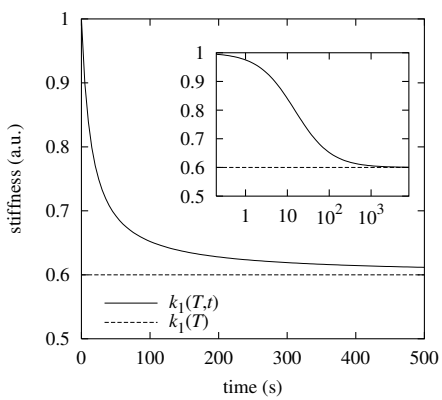

Figure 6. Variation of the stiffness k_1 with time. The inset shows the same function with a logarithmic time axis – only after about 10^3 s the final stiffness is reached.

Note that, due to the factor $k_1(T)$ in the denominator of Eq. (9), the change of stiffness is faster for higher temperatures. In the hot limit, changes take place very rapidly, whereas in the cold limit changes are extremely slow.

Finally, we note that the adaption/relaxation of $k_1(T,t)$ to the desired $k_1(T)$ value follows the above equations in all cases except when the temperature is going down and $k_1(T) > k_1(T,t)$. In that situation the contacts freeze rapidly and thus have to become strong as fast as the system cools down.

3.5 Cohesion dependence on stiffness and friction

The cohesive properties of a particle contact depend on the temperature, in so far that a melted contact should have weak tensile and compressive strength. Therefore, we couple the cohesive parameter k_c to the magnitude of $k_1(T,t)$, which decreases with temperature increasing. In addition, in order to take into account a reduced tensile strength of a soft contact with weak deformation and thus small overlap, the cohesion is directly related to the stiffness $k_2(\delta_{\text{max}})$:

$$k_c(T,t,\delta_{\text{max}}) = \frac{k_1(T,t)}{k_1} \frac{k_2(\delta_{\text{max}})}{k_2} k_c \ . \qquad (10)$$

This is an arbitrary choice for the temperature dependence of the cohesive force strength k_c, but as long as no detailed experimental results are available, we stick to this empirical law.

3.6 Tangential Contact Model

The force in tangential direction is implemented in the spirit of Cundall and Strack (Cundall and Strack 1979; Luding 2004), who introduced a tangential spring in order to account for static friction. Various authors have used this idea and numerous variants were implemented, see (Brendel and Dippel 1998; Luding 2004) for a summary and discussion, and the paper by Luding et al. in this volume for a description of the tangential spring implementation.

In brief, the tangential force is coupled to the normal force via Coulomb's law, i.e. $f^t \leq \mu f^n$, where for the limit case one has sliding friction and for the case of small forces f^t, one has static Coulomb friction. As a consequence of the cohesion force in normal direction, attractive forces are possible so that Coulomb's law has to be modified

$$f^t \leq \mu(f^n - f_{\text{min}}) \ , \qquad (11)$$

with the minimum (maximum attractive) force

$$f_{\text{min}} = -\frac{k_2(\delta_{\text{max}}) - k_1(T,t)}{1 + k_2(\delta_{\text{max}})/k_c(T,t,\delta_{\text{max}})} \delta_{\text{max}} \ . \qquad (12)$$

Thus the tangential force is related to the normal force relative to the point of cohesion-failure. Note that this changed force law can lead to a stable equilibrium of the solid also at $f^n \approx 0$ and activated tangential static friction.

3.7 Temperature dependence in tangential direction

In parallel to the change of normal stiffness, the tangential stiffness is always kept in a constant ratio α to k_2 so that

$$k_t = \alpha k_2(\delta_{\text{max}}) \ , \qquad (13)$$

since the stiffness in tangential direction is based on the same arguments as the material stiffness in normal direction.

The friction is coupled to the temperature dependent value of the stiffness $k_1(T,t)$, because friction

should not be present in a liquid at large enough temperatures, so that

$$\mu(T,t) = \frac{k_1(T,t)}{k_1}\mu \ . \tag{14}$$

Thus friction is modified together with the changes in normal direction. No new ideas are introduced for the tangential forces.

4 RESULTS

Now, the sintering model can be applied to the sintering process of a particulate material sample (Luding, Manetsberger, and Müllers 2004). The material is initially a loose powder and first has to be prepared at low temperature from time $t = 0$ to time t_{heat}, see Fig. 7. The preparation takes place with isotropic external pressure $p = 100$, where pressure is measured in units of $\mathrm{N\,m^{-1}}$ due to the two-dimensional nature of the model, and a pressure of $p = 100$ corresponds to $f^n \approx 2ap$, as rough estimate. The other system parameters are summarized in (Luding, Manetsberger, and Müllers 2004).

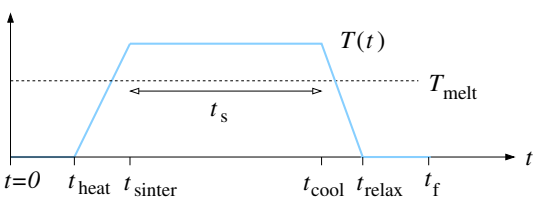

Figure 7. Schematic plot of the temperature variation during simulation in a preparation-heating-sintering-cooling-relaxation cycle.

4.1 Sample preparation

The preparation of the sample consists of an initial relaxation period at constant temperature $T = 80^0$C until time t_{heat}, when the system is heated up to $T = 140^0$C between time t_{heat} and t_{sinter}. During the sintering time t_s, the system is allowed to sinter with a much shorter relaxation time, $t_0 = 0.1$ instead of $t_0 = 10^3$ as used during the rest of the process. This 'trick' allows for a long time sintering simulation while keeping the simulation time small. During sintering, the time axis should be stretched by a factor of 10^4 in order to obtain the real-time behavior. At the end of the sintering process, at time t_{cool}, the sample is slowly cooled down and, at time t_{relax} allowed to relax at constant temperature until time t_{f}. Here, the times $t_{\text{heat}} = 0.2$, $t_{\text{sinter}} - t_{\text{heat}} = 0.1$, different sintering times $t_s := t_{\text{cool}} - t_{\text{sinter}}$, $t_{\text{relax}} - t_{\text{cool}} = 0.1$, and $t_{\text{f}} - t_{\text{relax}} = 0.1$ were used.

4.1.1 Density

The longer the sintering time t_s, the lower the value of k_1 gets. For short sintering time, the lowest values are never reached, because the system is cooled down before the sintering is finished. At the end of the sintering time, k_1 is increasing during the cooling process of the sample and reaches its inital value. However, the melting and sintering of the contacts is *not reversed*, as becomes evident when plotting the volume fraction ν in Fig. 8.

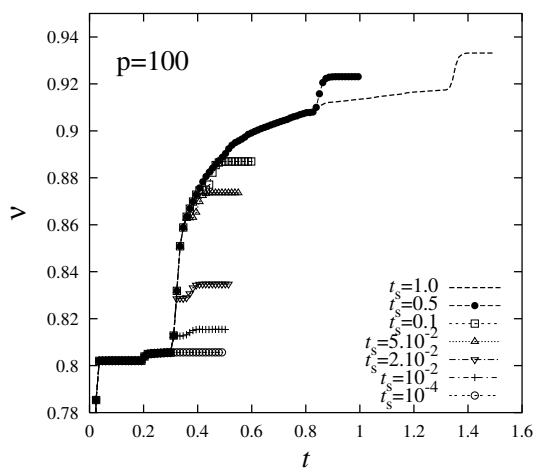

Figure 8. Material density ν as function of time for simulations with $N = 300$ particles and side stress $p = 100$.

The initial preparation step leads to a rather low density of $\nu \approx 0.8$. At time t_{heat}, the relaxed sample is heated up and, at the same time, the wall friction is switched off. The latter has an immediate effect, a slight increase in density is possible due to reorganizations. The increased temperature becomes only effective at time t_{sinter}, when the relaxation time t_0 is decreased in order to accelerate the evolution of the system. Note that the increase in density due to the sintering seemingly appears quite rapid – due to the quenched time axis during sintering.

In summary, longer sintering and larger confining pressures (data not shown) lead to higher densities of the sintered sample. Through test simulations with different parameters, we verified that the increase in density is only partially due to the contact model, but also is caused by reorganizations in the sample. A small thermal expansion of the particles, thus, does not affect the results.

4.2 Material properties

The samples prepared via the procedure described above are now tested via a compression test, where the vertical confining pressure is slowly increased. More data and also a vibration test are provided in

(Luding, Manetsberger, and Müllers 2004).

The compression test is a variant of the bi-axial compression frequently used in soil- or powder mechanics. A given compressive stress in one direction ($p = \sigma_{xx}$) is kept constant by moving the right, vertical wall, if neccessary. The other confining stress σ_{zz} is increased by moving the vertical wall down in a defined way, where compression is defined positive, $\epsilon_{zz}(t) > 0$. The density evolution of a sample with $N = 300$ particles is plotted against the strain for various sintering times in Fig. 9.

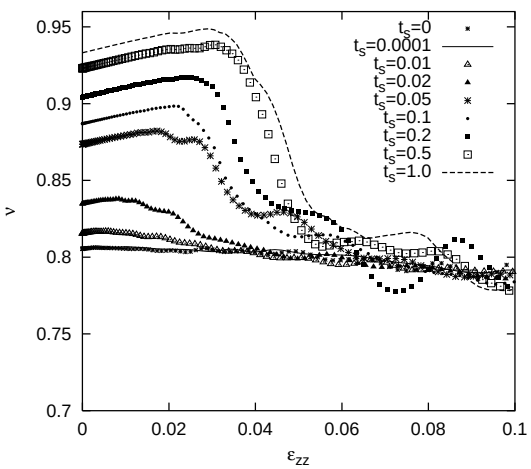

Figure 9. Material density as function of the vertical strain for samples prepared with different sintering times t_s and pressure $p_{\mathrm{w}} = 100$.

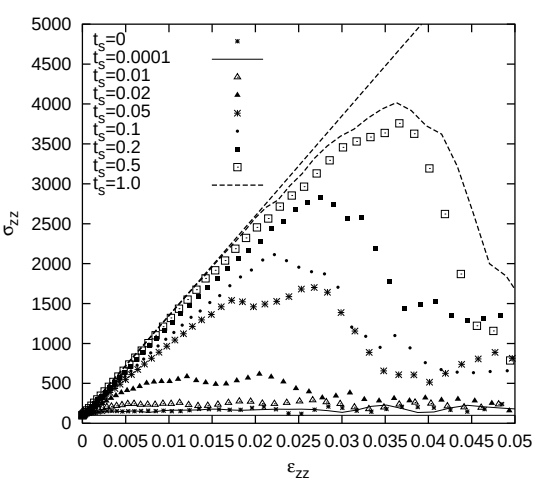

Figure 10. Vertical stress as function of the vertical strain for samples prepared with different sintering times t_s and pressure $p_{\mathrm{w}} = 100$.

The vertical stress is plotted against the strain in Fig. 10. With increasing strain, the vertical stress in the sample increases and the material fails at a certain maximal stress and critical strain (Luding, Manetsberger, and Müllers 2004). The material stiffness (dashed line in Fig. 10) is increased by about a factor of two when the confining stress is increased by a factor of ten. In summary, the critical strain and stress where the material fails increase with increasing confining pressure, sintering time and system size.

One snapshot from a compression test for a long sintering time, $N = 300$ and $p = 10$ is presented in Fig. 11. Gaps (cracks) between the parts of the sample have opened and fragments are evident. This is only a representative example for the compression test; a more detailed study of the fracture behavior, sample-size- and sintering-time-dependence is far from the scope of this study.

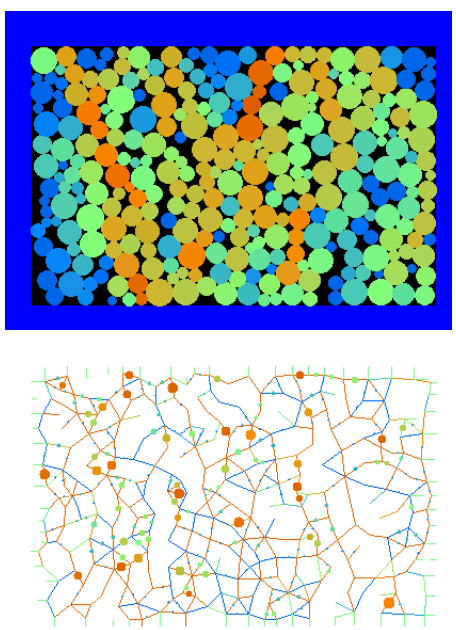

Figure 11. Snapshot of a compression test with $N = 300$ and $p = 10$, at deformation $\varepsilon_{zz} = 0.04$ and $t_s = 1.0$. (Top) The circles are the particles with the greyscale coding the average stress; dark and light correspond to small and large stresses. (Bottom) The lines are contacts; cracks are where no lines are drawn anymore. The small solid circles denote the tangential forces, with their size proportional to its magnitude.

5 CONCLUSION

In summary, a discrete contact model for the sintering of particulate materials was introduced and some material samples were sintered for different times. Then they were tested with respect to their anisotropic load strength: Longer sintering and stronger confining pressure systematically increases the density and the strength of the material. Depending on the sintering duration, either isolated particles (short sintering), fragments or a single solid block of material (long sintering at large pressure) could be produced. Further research includes more model tests via a comparison with experimental data, extension of the model

to three dimensions – the model was designed such that this should be straightforward. The last missing ingredients in the model, like rolling- and torsion-resistance will make the model even more realistic. Note, however, that already the model presented here increased the amount of computation necessary for each contact by some factor.

ACHNOWLEDGEMENTS

The author thanks M. Lätzel, K. Manetsberger, Johannes Müllers, J. Tomas, S. Diebels, H. Besserer, and G. A. D´Addetta for discussions and acknowledges financial support by the Deutsche Forschungsgemeinschaft (DFG) and by the DaimlerChrysler research division.

REFERENCES

Allen, M. P. and D. J. Tildesley (1987). *Computer Simulation of Liquids*. Oxford: Oxford University Press.

Brendel, L. and S. Dippel (1998). Lasting contacts in molecular dynamics simulations. In H. J. Herrmann, J.-P. Hovi, and S. Luding (Eds.), *Physics of Dry Granular Media*, Dordrecht, pp. 313. Kluwer Academic Publishers.

Cundall, P. A. and O. D. L. Strack (1979). A discrete numerical model for granular assemblies. *Géotechnique 29*(1), 47–65.

DeLo, D. P., R. E. Dutton, and S. L. Semiatin (1999). A comparison of discrete element model prediction to observation of metal powder consolidation. *Scripta Materialia 40*(10), 1103–1109.

Herrmann, H. J., J.-P. Hovi, and S. Luding (Eds.) (1998). *Physics of dry granular media - NATO ASI Series E 350*, Dordrecht. Kluwer Academic Publishers.

Jagota, A. and P. R. Dawson (1990). Simulation of the viscous sintering of 2 particles. *Journal of the American Ceramic Society 73*(1), 173–177.

Luding, S. (1997). Surface waves and pattern formation in vibrated granular media. In *Powders & Grains 97*, Amsterdam, pp. 373–376. Balkema.

Luding, S. (1998). Collisions & contacts between two particles. In H. J. Herrmann, J.-P. Hovi, and S. Luding (Eds.), *Physics of dry granular media - NATO ASI Series E350*, Dordrecht, pp. 285. Kluwer Academic Publishers.

Luding, S. (2004). Micro-macro transition for anisotropic, periodic, elastic solids. in preparation.

Luding, S., K. Manetsberger, and J. Müllers (2004). A disrete model for long time sintering. J. Mech. Phys. Solids, in press.

Olevsky, E. A. (1998). Theory of sintering: from discrete to continuum. *Materials Science and Engineering R23*, 41–100.

Redanz, P. and N. A. Fleck (2001). The compaction of a random distribution of metal cylinders by the discrete element method. *Acta Materialia 49*, 4325–4335.

Riedel, H. and B. Blug (2001). A comprehensive model for solid state sintering and its application to silicon carbide. In T.-J. Chuang and J. W. Rudnicki (Eds.), *Multiscale deformation and fracture in materials and structures, the James R. Rice 60th anniversary volume, Solid mechanics and its application - Vol. 84*, Dordrecht, pp. 49–70. Kluwer Academic Publishers.

Sadd, M. H., Q. M. Tai, and A. Shukla (1993). Contact law effects on wave propagation in particulate materials using distinct element modeling. *Int. J. Non-Linear Mechanics 28*(2), 251.

Schwedes, J. (1968). *Fließverhalten von Schüttgütern in Bunkern*. Weinheim: Verlag Chemie.

Tomas, J. (2000). Particle adhesion fundamentals and bulk powder consolidation. *KONA 18*, 157–169.

Vermeer, P. A., S. Diebels, W. Ehlers, H. J. Herrmann, S. Luding, and E. Ramm (Eds.) (2001). *Continuous and Discontinuous Modelling of Cohesive Frictional Materials*, Berlin. Springer. Lecture Notes in Physics 568.

Walton, O. R. and R. L. Braun (1986). Viscosity, granular-temperature, and stress calculations for shearing assemblies of inelastic, frictional disks. *Journal of Rheology 30*(5), 949–980.

Zhu, C. Y., A. Shukla, and M. H. Sadd (1991). Prediction of dynamic contact loads in granular assemblies. *J. of Applied Mechanics 58*, 341.